Journal Pre-proofs

IR780 loaded sulfobetaine methacrylate-functionalized albumin nanoparticles aimed for enhanced breast cancer phototherapy

Cátia G. Alves, Duarte de Melo-Diogo, Rita Lima-Sousa, Ilídio J. Correia

PII: S0378-5173(20)30330-6
DOI: https://doi.org/10.1016/j.ijpharm.2020.119346
Reference: IJP 119346

To appear in: *International Journal of Pharmaceutics*

Received Date: 7 January 2020
Revised Date: 8 April 2020
Accepted Date: 16 April 2020

Please cite this article as: C.G. Alves, D. de Melo-Diogo, R. Lima-Sousa, I.J. Correia, IR780 loaded sulfobetaine methacrylate-functionalized albumin nanoparticles aimed for enhanced breast cancer phototherapy, *International Journal of Pharmaceutics* (2020), doi: https://doi.org/10.1016/j.ijpharm.2020.119346

IR780 loaded sulfobetaine methacrylate-functionalized albumin nanoparticles aimed for enhanced breast cancer phototherapy

Cátia G. Alves[1,a], Duarte de Melo-Diogo[1,a,*], Rita Lima-Sousa[a], Ilídio J. Correia[a,b,*]

[1] These authors contributed equally to this article.

[a] CICS-UBI – Centro de Investigação em Ciências da Saúde, Universidade da Beira Interior, 6200-506 Covilhã, Portugal.

[b] CIEPQPF – Departamento de Engenharia Química, Universidade de Coimbra, Rua Sílvio Lima, 3030-790 Coimbra, Portugal.

[*] Corresponding Authors E-mail: demelodiogo@fcsaude.ubi.pt (Duarte de Melo-Diogo); icorreia@ubi.pt (Ilídio J. Correia).

Abstract

New insights about nanomaterials' biodistribution revealed their ability to achieve tumor accumulation by taking advantage from the dynamic vents occurring in tumor's vasculature. This paradigm-shift emphasizes the importance of extending nanomaterials' blood circulation time to enhance their tumor uptake. The classic strategy to improve nanomaterials' stability during circulation relies on their functionalization with poly(ethylene glycol). However, recent reports have been showing that PEGylated nanomaterials can suffer from the accelerated blood clearance phenomenon, emphasizing the importance of developing novel coatings for functionalizing the nanomaterials. To address this limitation, the modification of natural carriers' surface to enhance their stability appears to be a promising strategy. Herein, sulfobetaine methacrylate (SBMA)-functionalized bovine serum albumin (BSA) was synthesized for the first time to investigate the capacity of this modification to improve the resulting nanoparticles' physicochemical properties, colloidal stability and *in vitro* performance. This novel polymer was then employed in the formulation of nanoparticles loaded with IR780 for application in breast cancer phototherapy (IR/SBMA-BSA NPs). When compared to their non-functionalized equivalents, the IR/SBMA-BSA NPs presented a neutral surface charge and a higher stability in biologically relevant media. Due to these features, the IR/SBMA-BSA NPs could achieve a 1.9-fold greater uptake by breast cancer cells than IR/BSA NPs. Furthermore, the IR/SBMA-BSA NPs were cytocompatible towards normal cells and reduced breast cancer cells' viability up to 42 %. The phototherapy mediated by IR/SBMA-BSA NPs could further decrease cancer cells' viability to about 12 %. Overall, the IR/SBMA-BSA NPs have enhanced features that propel their application in breast cancer phototherapy.

Keywords: Albumin nanoparticles, Breast cancer, IR780, Photothermal therapy, Polymer functionalization, Zwitterionic coatings

Abbreviation List

^{1}H NMR - Proton Nuclear Magnetic Resonance

ABC - Accelerated Blood Clearance

ANOVA - Analysis of Variance

BSA – Bovine Serum Albumin

DLS - Dynamic Light Scattering

DMEM-F12 - Dulbecco's Modified Eagle's Medium-F12

DTT - DL-Dithiothreitol

EE - Encapsulation Efficiency

EPR - Enhanced Permeability and Retention

FBS - Fetal Bovine Serum

FTIR - Fourier Transform Infrared Spectroscopy

IR/BSA NPs – IR780 loaded BSA nanoparticles

IR/SBMA-BSA NPs – IR780 loaded SBMA-*g*-BSA nanoparticles

MCF-7 - Michigan Cancer Foundation-7

NHDF - Normal Human Dermal Fibroblasts

NIR - Near Infrared

ns - Non-significant

PBS - Phosphate Buffered Saline

PDI - Polydispersity Index

PEG - Poly(ethylene glycol)

SBMA - [2-(methacryloyloxy)ethyl]dimethyl-(3-sulfopropyl)ammonium hydroxide

SBMA-*g*-BSA – BSA grafted with SBMA

S.D. - Standard Deviation

TEM - Transmission Electron Microscopy

1. Introduction

Phototherapies mediated by nanomaterials have been revealing promising results for cancer therapy (de Melo-Diogo et al., 2017b). This novel therapeutic modality takes advantage from the ability of nanomaterials to passively accumulate at the tumor site (Blanco et al., 2015). Subsequently, this zone is exposed to near infrared (NIR; 750-1000 nm) light, and the tumor homed nanomaterials absorb it, generating a temperature increase (photothermal therapy) and/or reactive oxygen species (ROS, photodynamic therapy) (Alves et al., 2018). Considering that the NIR radiation has minimal/insignificant interactions with the biological components (*e.g.* water, melanin, collagen), the phototherapies mediated by NIR responsive nanomaterials can potentially perform a spatio-temporal controlled therapy with minimal side effects (de Melo-Diogo et al., 2017b).

Despite nanomaterials' potential for cancer treatment, a recent exhaustive literature analysis has disclosed that less than 1 % of the nanoparticles' injected dose reaches the tumor (Wilhelm et al., 2016). Such reality may be explained by the fact that nanomaterials' size has been highly considered as a key parameter mediating nanomedicines' tumor uptake. In fact, nanomaterials can accumulate in the tumor zone by extravasating through the leaky tumor vasculature, which has fenestrae with variable sizes (200-1200 nm) (de Melo-Diogo et al., 2017b; Hobbs et al., 1998). However, new insights into nanomaterials' biodistribution revealed that they can also benefit from the dynamic vents (also termed as eruptions) occurring on the tumor vasculature to accomplish tumor accumulation (Matsumoto et al., 2016). Based on this new mechanism, researchers have been modulating nanomaterials' surface properties to increase their blood circulation, leading to an improved tumor uptake (Matsumoto et al., 2016).

The functionalization of nanomaterials' surface with poly(ethylene glycol) (PEG) is the classic strategy employed to improve their blood circulation time (Otsuka et al., 2012; Yan et al., 2019). In fact, PEGylated nanomaterials exhibiting a long blood circulation can achieve a high tumor uptake (Liu et al., 2011; Zhou et al., 2010). However, several studies have demonstrated that systemically administered PEGylated nanomaterials can induce immunogenic reactions (Abu Lila et al., 2013a; d'Avanzo et al., 2019). In brief, at the time of the first intravenous

administration of PEG-nanoparticles, anti-PEG antibodies are formed. These anti-PEG antibodies will then mediate the rapid clearance of the PEG-nanoparticles in subsequent administrations, rendering them ineffective since these will not reach the target site (Abu Lila et al., 2013a; d'Avanzo et al., 2019). This behaviour is known as the accelerated blood clearance (ABC) phenomenon. The magnitude of the ABC phenomenon depends on multiple factors related to the nanomaterials' intrinsic properties (*e.g.* type of nanomaterial, PEG density, PEG molecular weight) and to their administration protocol (*e.g.* administration schedule, dose, route) (Abu Lila et al., 2013a; Abu Lila et al., 2013b; d'Avanzo et al., 2019; Shiraishi et al., 2013; Xu et al., 2010). Nevertheless, these findings should still motivate the development of other nanomaterials' functionalization strategies.

To surpass this bottleneck, the use of natural structures, with long blood circulation times, to formulate nanomaterials is an attractive approach. Albumin based carriers meet this criterion and are also highly biocompatible and easy to prepare (An and Zhang, 2017). For instance, the coating of porous silicon nanoparticles with albumin increased their blood circulation half-life from about 29 min to 4.4 h (Xia et al., 2013). Nevertheless, PEG coated nanomaterials can still display greater blood circulation times ($t_{1/2} \approx 22$ - 34 h) (Prencipe et al., 2009; Sheng et al., 2009). In this way, the modification of albumin-based carriers' surface to display an improved stability could possibly potentiate their blood circulation time and hence their tumor uptake (Muro et al., 2010; Shutava et al., 2018).

In this work, and to the best of our knowledge, sulfobetaine methacrylate (SBMA)-modified bovine serum albumin (BSA) was synthesized for the first time to investigate the capacity of this modification to improve the resulting nanoparticles' physicochemical properties, colloidal stability and *in vitro* performance. This novel polymer was then employed in the formulation of nanoparticles loaded with IR780 for application in breast cancer phototherapy. SBMA was grafted into albumin since it can reduce protein adsorption (Chang et al., 2006; Ladd et al., 2008; Peng et al., 2020), and thus may possibly enhance nanomaterials' stability during circulation. For instance, Men *et al.* verified that poly(SBMA)-based nanogels can achieve a longer blood circulation half-life than their PEGylated equivalents,

leading to an up to 4.65-fold higher tumor uptake (10.7 % *vs.* 2.3 % ID/g of tumor) (Men et al., 2018). Furthermore, nanomaterials with SBMA brushes are not reported to suffer from the ABC phenomenon (Men et al., 2018). As importantly, the direct conjugation of SBMA into albumin is a simpler process when compared to the polymerization of SBMA on nanomaterials' surface (Ibrahim et al., 2017; Lou et al., 2017). Then, SBMA-*g*-BSA nanoparticles incorporating a NIR responsive small molecule with photothermal and photodynamic capabilities (IR780) were prepared (IR/SBMA-BSA NPs) using the nanoprecipitation method (Alves et al., 2018; Leitão et al., 2020). The results obtained revealed that IR/SBMA-BSA NPs present a suitable size distribution for application in cancer therapy with an average size of 96.1 ± 8.1 nm and a spherical morphology. When compared to the non-functionalized BSA nanoparticles loaded with IR780 (IR/BSA NPs), the IR/SBMA-BSA NPs presented a neutral surface charge and an increased stability in biologically relevant media. Due to these features, the IR/SBMA-BSA NPs could display a 1.9-fold greater uptake by MCF-7 cells than IR/BSA NPs. The photothermal capacity of IR/SBMA-BSA NPs was also investigated, being verified that the nanostructures generate a temperature increase upon interaction with NIR light. In the cell culture studies, the IR/SBMA-BSA NPs were cytocompatible towards normal cell lines. However, these induced a dose- and time-dependent cytotoxic effect on breast cancer cells. IR/SBMA-BSA NPs therapeutic capacity was further increased when the cells were exposed to NIR radiation.

2. Materials and Methods

2.1. Materials

IR780 iodide, resazurin, DL-Dithiothreitol (DTT), Dulbecco 's Modified Eagle 's Medium F12 (DMEM-F12), [2-(methacryloyloxy)ethyl]dimethyl-(3-sulfopropyl)ammonium hydroxide (SBMA), and trypsin were acquired from Sigma-Aldrich (Sintra, Portugal). Bovine Serum Albumin was obtained from Amresco (Pennsylvania, EUA). Acetone, Triton X-100, and methanol were bought from Fisher Scientific (Oeiras, Portugal). Michigan Cancer Foundation-7 (MCF-7) cell line was acquired from ATCC (Middlesex, UK) and Normal Human Dermal Fibroblast (NHDF) from Promocell (Heidelberg, Germany). Cell culture

plates and T-flasks were purchased from Thermo Fisher Scientific (Porto, Portugal). Fetal Bovine Serum (FBS) was obtained from Biochrom AG (Berlin, Germany). Water used in all experiments was double deionized (0.22 μm filtered, 18.2 M Ω cm).

2.2. Methods

2.2.1. SBMA-*g*-BSA synthesis and characterization

The synthesis of SBMA-*g*-BSA was performed through a Michael addition by adapting the protocol previously described by Venault and co-workers (Venault et al., 2014). In brief, BSA (250 mg) and SBMA (194 mg) were dissolved in water (a molar excess of SBMA to the primary amine and thiol groups of BSA was used). Afterwards, the pH of the solution was adjusted to 12 using NaOH (1 M) and the solution was left to stir at 37 °C for 24 h. Then, this solution was dialyzed (14 kDa molecular weight cut-off) against water for 2 days and the recovered solution was freeze-dried (ScanVac CoolSafe, LaboGene ApS, Lynge, Denmark), yielding SBMA-*g*-BSA. The successful synthesis of SBMA-*g*-BSA was confirmed by Fourier transform infrared spectroscopy (FTIR) using a Nicolet iS10 spectrometer (Thermo Scientific Inc., MA, USA) and by Proton nuclear magnetic resonance (^{1}H NMR) using a Brüker Avance III 400 MHz spectrometer (Brüker Scientific Inc., NY, USA). For the ^{1}H NMR experiments, SBMA, BSA and SBMA-*g*-BSA were analysed at 298 K in 9:1 (v/v) H_2O/D_2O. MNova software (Mestrelab Research, SL, Santiago de Compostela, Spain) was used to process and analyse the acquired spectra.

2.2.2. Formulation of IR/SBMA-BSA NPs

IR780 loaded SBMA-*g*-BSA nanoparticles (IR/SBMA-BSA NPs) were formulated using the nanoprecipitation technique (Alves et al., 2019). Initially, SBMA-*g*-BSA (5 mg) and DTT (386 μg) were added to 5 mL of PBS and then were left to react for 20 min under stirring. Afterwards, IR780 (250 μg) in acetone (1 mL) was added dropwise to the polymer-DTT solution during 20 min at RT. Then, this solution was recovered and dialyzed (14 KDa molecular weight cut-off) against water for 90 min, yielding IR/SBMA-BSA NPs. As a control, IR780 loaded BSA

nanoparticles (IR/BSA NPs) were also prepared using the above described method but using BSA instead of SBMA-*g*-BSA.

2.2.3. Physicochemical characterization of IR/SBMA-BSA NPs

The size distribution of the produced NPs was determined by Dynamic Light Scattering (DLS) using a ZetaSizer NanoZS (Malvern Instruments Ltd., Worcestershire, UK) at 25 °C. Furthermore, the variation of nanoparticles' size overtime when dispersed in PBS (pH 7.4; 10 mM of Na_2HPO_4) and cell culture medium (DMEM-F12 supplemented with 0, 10 and 20 % (v/v) of FBS) was also analysed. The zeta potential of the nanoformulations in water, PBS (pH 7.4) at 5 and 10 mM (of Na_2HPO_4) and DMEM-F12 medium with 0, 10 and 20 % (v/v) of FBS was also determined using the ZetaSizer. To evaluate the morphology of the nanoparticles, these were stained with phosphotungstic acid (2 % (w/v)) before being analysed in a Hitachi-HT7700 transmission electron microscope (TEM, Hitachi Ltd., Tokyo, Japan), operated at an accelerating voltage of 100 kV. Samples' UV-Vis-NIR absorption spectrum was acquired by using an Evolution 201 spectrophotometer (Thermo Scientific Inc.). For this purpose, IR/SBMA-BSA NPs dispersed in water, PBS (pH 7.4; 10 mM of Na_2HPO_4) and cell culture medium with 10 % of FBS were analysed. The encapsulation efficiency (EE) of IR780 in the IR/SBMA-BSA NPs was determined by analysing the samples' absorbance at 780 nm in a water:methanol (1:1 (v/v)) solution, using a method previously reported by our group (Alves et al., 2019). The photothermal capacity of IR/SBMA-BSA NPs was determined by exposing the nanomaterials to NIR radiation (808 nm, 1.7 W cm^{-2}) and recording the temperature variations using a thermocouple thermometer (de Melo-Diogo et al., 2017a).

2.2.4. Cytocompatibility of IR/SBMA-BSA NPs

IR/SBMA-BSA NPs cytocompatibility towards MCF-7 cells and NHDF was assessed using the resazurin method as we have previously described (Lima-Sousa et al., 2018). To perform these assays, cells were cultured in DMEM-F12 medium supplemented with 10 % (v/v) of FBS and 1 % (v/v) of streptomycin/gentamycin in a humified incubator (37 °C; 5 % of CO_2). To evaluate

IR/SBMA-BSA NPs cytocompatibility, MCF-7 cells and NHDF were cultured in 96-well plates at a density of 1 × 10^4 cells per well. After 24 h, cells were incubated with medium containing different concentrations of IR/SBMA-BSA NPs (0.5 - 5 μg mL^{-1} of IR780 equivalents) during 24 and 48 h. Afterwards, cells were incubated with fresh medium containing 10 % (v/v) of resazurin during 4 h in the dark (37 °C, 5% CO_2). Finally, the fluorescence of resorufin was quantified to assess cells' viability by using excitation and emission wavelengths of 560 and 590 nm, respectively, using a Spectramax Gemini EM spectrofluorometer (Molecular Devices LLC, California, USA). Non treated cells were used as the negative control (K-) while cells treated with ethanol 70 % were used as the positive control (K+).

2.2.5. Uptake of IR/SBMA-BSA NPs by MCF-7 cells

The uptake of IR/SBMA-BSA NPs by MCF-7 cells was determined as previously described by our group (Reis et al., 2019). In brief, MCF-7 cells (1 × 10^4 cells/well) were seeded in 96-well plates, and after 24 h, cells were incubated with fresh medium (DMEM-F12 supplemented with 0, 10 or 20 % (v/v) of FBS) containing IR/SBMA-BSA NPs or IR/BSA NPs at a concentration of 1 μg mL^{-1} (of IR780 equivalents) during 4 h. Then, cells were washed with ice-cold Krebs Ringer Buffer in order to remove the non-internalized nanoparticles. Subsequently, cells were incubated with a lysis solution (1 % (v/v) of Triton X-100 in Krebs Buffer) under orbital stirring for 30 min. Finally, the IR780 fluorescence in the cell lysate was quantified in a spectrofluorometer using excitation and emission wavelengths of 780 and 800 nm, respectively. The control was performed with cells only incubated with Krebs Buffer.

2.2.6. Phototherapeutic effect mediated by IR780/SBMA-BSA NPs

The phototherapeutic effect mediated by IR/SBMA-BSA NPs was determined as we previously described (Lima-Sousa et al., 2018). In brief, MCF-7 cells were seeded in 96-well plates at a density of 1 x 10^4 cells per well. After 24 h, the medium was replaced by fresh medium containing different concentrations of IR/SBMA-BSA NPs (1, 2 and 5 μg mL^{-1} of IR780 equivalents). After 4 h, the cells

were irradiated with NIR light (808 nm, 1.7 W cm^{-2}) for 5 min. After 24 h of incubation, the medium was replaced by fresh medium containing resazurin (10 % (v/v)) and the cells' viability was determined as described above.

2.2.7. Statistical analysis

The statistical analysis of two groups was performed using the unpaired *t-student* test. Multiple groups comparison was performed by one-way analysis of variance (ANOVA) with the Student-Newman-Keuls test. A *p*-value <0.05 was considered statistically significant. All data are represented as the mean ± standard deviation (S.D.). Data analysis was performed in GraphPad Prism v6.0 (Trial version, GraphPad Software, CA, USA).

3. Results and Discussion

3.1. Synthesis and characterization of SBMA-*g*-BSA

The synthesis of SBMA-*g*-BSA was performed by a simple method (Figure 1(A)). The FTIR spectrum of SBMA showed its S=O stretch (at 1036 and 1235 cm^{-1}) and C=O stretch (at 1715 cm^{-1}) characteristic peaks (Figure 1(B)). In turn, the FTIR spectrum of BSA displayed several peaks belonging to O-H, C-H and C=O vibrations (Figure 1(B)). In the FTIR spectrum of SBMA-*g*-BSA, the characteristic peaks of the BSA functional groups are present as well as the S=O stretch peaks of SBMA (Figure 1(B) and (C)). Furthermore, the ^{1}H NMR spectrum of SBMA displays a peak at δ ≈ 3.22 ppm corresponding to the -N($C\mathbf{H_3}$)$_2$- methyl protons - Figure 1(D). Furthermore, peaks at δ ≈ 3.58 ppm and δ ≈ 2.98 ppm belonging to the -$C\mathbf{H_2}N(CH_3)_2$- and -$C\mathbf{H_2}SO_3$ methylene protons are also present (Zou et al., 2020). In turn, the ^{1}H NMR spectrum of SBMA-*g*-BSA presents the characteristic methyl and methylene protons of SBMA (δ ≈ 3.22; 3.58 and 2.98 ppm Figure 1(F)) as well as those belonging to BSA (Figure 1(E); (Spence et al., 2011)). Considering that non-grafted SBMA is removed through dialysis, these results confirm the successful synthesis of SBMA-*g*-BSA.

3.2. Formulation and characterization of IR/SBMA-BSA and IR/BSA NPs

In order to improve the natural carrier properties of BSA, this protein was modified with SBMA yielding SBMA-*g*-BSA. Then, a simple nanoprecipitation method was used to produce IR780 loaded SBMA-*g*-BSA nanoparticles (IR/SBMA-BSA NPs) due to its simplicity and reproducibility (Figure 2(A)) (Pais-Silva et al., 2017). The DLS analysis revealed that IR/SBMA-BSA NPs have an average size of 96.1 ± 8.1 nm and a low PDI of 0.181 (Figure 2(B); n = 3, batch triplicates). As control, IR780 loaded BSA nanoparticles (IR/BSA NPs) were also prepared, displaying a similar size to that of IR/SBMA-BSA NPs (Figure S1(A)). Such indicates that the SBMA modification does not compromise the nanoparticle-forming capacity of BSA. Furthermore, the size of IR/SBMA-BSA NPs is also in agreement with that previously reported for other BSA-based nanoparticles (Bae et al., 2012; Kim et al., 2016) and it is within the range considered to be optimal for tumor accumulation (de Melo-Diogo et al., 2017b). TEM analysis (Figure 2(C)) revealed that IR/SBMA-BSA NPs display a spherical shape, a feature that was also observed in other IR780 loaded nanostructures prepared by the nanoprecipitation method (Alves et al., 2019; Lu et al., 2019; Pais-Silva et al., 2017). As importantly, spherical shaped nanomedicines have been associated to an increased uptake by cancer cells (Chithrani, 2010; Zhang et al., 2008).

The zeta potential of IR/SBMA-BSA NPs was determined to be -9.6 ± 0.3 mV, while that of IR/BSA NPs was -12.3 ± 0.4 mV (in PBS 10 mM pH 7.4; n = 3, batch triplicates) – Table 1. The solutions' ionic strength can also influence nanoparticles' zeta potential (Nikam et al., 2014). In this way, the zeta potential of IR/SBMA-BSA NPs and IR/BSA NPs in different media was also determined (Table 1). As expected, in biologically relevant media, the IR/SBMA-BSA NPs presented a more neutral surface charge when compared to those displayed by IR/BSA NPs (Table 1). The difference in the surface charge of IR/SBMA-BSA NPs can be justified by the SBMA grafting into BSA since SBMA coatings are neutrally charged (Chen et al., 2014; Venault et al., 2014). As importantly, the zeta potentials of IR/SBMA-BSA NPs are within the so-called neutral charge range (-10 to +10 mV), which has been described as optimal in the literature (de Melo-Diogo et al., 2017b).

IR/SBMA-BSA NPs had an IR780 encapsulation efficiency of 50.7 ± 3.3 %. The encapsulation of IR780 in other polymer-based nanoparticles and micelles also

yielded similar results (Alves et al., 2019; Jiang et al., 2015). Moreover, the loading of IR780 into the IR/SBMA-BSA NPs enhanced the water solubility of this NIR dye by 63-fold (from 0.4 to 25.35 μg mL^{-1}) (Jiang et al., 2015). In this way, the loading of IR780 into the IR/SBMA-BSA NPs addresses the low water solubility of IR780, which is a major drawback of this NIR dye.

Lastly, the stability of the IR/SBMA-BSA NPs overtime in PBS (10 mM pH 7.4; Figure 3(A)) and cell culture medium (DMEM-F12 supplemented with 0, 10 or 20 % (v/v) of FBS) was assessed (Figure 3(B) to (D)). Overall, IR/SBMA-BSA NPs maintained their size distribution overtime when incubated in all the solutions while the size of IR/BSA NPs could suffer stark variations. The size of IR/BSA NPs augmented by 14 % when these were dispersed in PBS (Figure 3(A)). On the other hand, when IR/BSA NPs were dispersed in cell culture medium without FBS, their size remained unaffected (Figure 3(B)). However, IR/BSA NPs dispersed in culture medium with 10 or 20 % of FBS suffered an increase in their size by up to 4-fold (Figure 3(C) and (D)). Such behaviour indicates that IR/BSA NPs may have a weaker stability and that interact with the proteins present on the culture medium. In fact, SBMA coatings can reduce protein adsorption, leading to an improvement in nanomaterials' stability during blood circulation (Dong et al., 2011; Men et al., 2018). In this way, the grafting of SBMA into BSA enabled the assembly of IR/SBMA-BSA NPs that display an improved stability.

3.3. NIR absorption and phototherapeutic capacity of IR/SBMA-BSA NPs

The ability of IR/SBMA-BSA NPs to interact with NIR light was then assessed by evaluating their NIR absorption (Figure 4(A)). As expected, free IR780 (dissolved in methanol) presented an absorption peak at 780 nm. The IR/SBMA-BSA NPs had their maximum NIR absorption at 792 nm (Figure 4(A)). This red-shift in IR780 absorption when encapsulated in SBMA-BSA NPs occurs due to the hydrophobic interactions established between the NIR dye and the aromatic moieties of the nanocarriers or due to alterations in solvents polarity (Pais-Silva et al., 2017). Due to this red shift, the IR/SBMA-BSA NPs absorbance at 808 nm is 1.04-times higher than that of free IR780 (at the same concentration of IR780 equivalents). This is of extreme importance since 808 nm laser light is generally used in cancer phototherapy (Kirui et al., 2010; Liu et al., 2017; Yuan et al., 2015).

As expected, the UV-Vis-NIR spectrum of IR/BSA NPs was similar to that of IR/SBMA-BSA NPs (Figure S1(B)), indicating that the SBMA-functionalization does not compromise the ability of these formulations to interact with NIR light.

Furthermore, the IR/SBMA-BSA NPs retained their NIR absorption overtime, even when dispersed in PBS (Figure 4(B)) or in DMEM-F12 supplement with 10 % of FBS (Figure 4(C)). Considering that free IR780 in aqueous solutions loses its optical properties overtime (Wang et al., 2016), the loading of IR780 into IR/SBMA-BSA NPs can enhance its optical stability.

To confirm their photothermal capacity, IR/SBMA-BSA NPs were irradiated with 808 nm laser light (808 nm, 1.7 W cm^{-2}) and the temperature variations were recorded (Figure 4(D)). Overall, IR/SBMA-BSA NPs produced a concentration- and time-dependent temperature increase when exposed to NIR light. At the maximum concentration tested (20 μg mL^{-1} of IR780 equivalents), the IR/SBMA-BSA NPs induced a temperature increase of about 13 °C after 2 min of irradiation, decreasing slightly afterwards. This phenomenon is attributed to the photodegradation of IR780, which has been extensively reported elsewhere (Guo et al., 2016; Wang et al., 2016). Still, the temperature variation achieved is sufficiently high to damage cancer cells (de Melo-Diogo et al., 2018; de Melo-Diogo et al., 2017b). As importantly, water exposed to NIR light (control) did not suffer a meaningful temperature variation ($\Delta T < 1.8$ °C). Such is in agreement with the low interaction of 808 nm with water and suggests the ability of IR/SBMA-BSA NPs to produce a therapeutic effect with high spatio-temporal resolution.

For instance, Lu *et al.* prepared IR780 loaded PEGylated zwitterionic nanoparticles that could produce a temperature increase of 10.8 °C after 2 min of irradiation (808 nm, 1.0 W cm^{-2}) at an IR780 concentration of 26.7 μg mL^{-1} (Lu et al., 2019). Herein, the IR/SBMA-BSA NPs generated a photoinduced heat of 13.2 °C after 2 min of irradiation (808 nm, 1.7 W cm^{-2}) using 20 μg mL^{-1} of IR780. Together, these results suggest that IR/SBMA-BSA NPs are also promising photothermal agents.

3.4. Cytocompatibility of IR/SBMA-BSA NPs

Before determining the phototherapeutic capacity of IR/SBMA-BSA NPs, their cytocompatibility towards breast cancer (MCF-7) and healthy human (NHDF) cells was assessed (Figure 5(A) and (B)). The IR/SBMA-BSA NPs did not induce cytotoxicity towards NHDF after an incubation period of 24 and 48 h, and up to a concentration of 5 μg mL^{-1} (of IR780 equivalents). In turn, IR/SBMA-BSA NPs produced a dose- and incubation time-dependent cytotoxicity on MCF-7 cells. Such effect may be related to the fact that IR780 predominantly accumulates in the mitochondria of MCF-7 cells and other types of cancer cells when compared to normal cells, thereby inducing a cytotoxic effect (Wang et al., 2014; Zhang et al., 2010). Pais-Silva and Jiang also reported a dose dependent cytotoxicity of IR780-loaded nanostructures towards MCF-7 cells (Jiang et al., 2015; Pais-Silva et al., 2017).

3.5. Uptake of IR/SBMA-BSA NPs by MCF-7 cells and phototherapeutic capacity

Then, the uptake of IR/SBMA-BSA NPs by MCF-7 cells was investigated (Figure 6(A) to (C); (Moreira et al., 2018; Reis et al., 2019)). For this analysis, IR/SBMA-BSA NPs and IR/BSA NPs were incubated using cell culture medium with 0, 10 or 20 % (v/v) of FBS.

When incubated in culture medium without FBS, the IR/SBMA-BSA NPs and IR/BSA NPs presented a similar internalization in MCF-7 cells (Figure 6(A)). In contrast, the uptake studies using culture medium with 10 % of FBS revealed that IR/SBMA-BSA NPs achieve a 1.58 ± 0.32-fold higher internalization in MCF-7 cells when compared to IR/BSA NPs (Figure 6(B)). This differential uptake was even more accentuated when the nanoformulations were incubated using culture medium with 20 % of FBS (Figure 6(C)). In this case, the uptake of IR/SBMA-BSA NPs by cancer cells was 1.89 ± 0.02-fold higher than that of IR/BSA NPs (Figure 6(C)).

In general, neutral- and positively- charged nanomaterials can achieve a higher cellular internalization as a result of interactions with the negatively charged components of cells' membrane (de Melo-Diogo et al., 2017b). In this way, the improved uptake of IR/SBMA-BSA NPs by MCF-7 cells can be explained by the

neutral surface charge of this formulation in the different media (as analysed in section 3.2.). The enhanced colloidal stability of IR/SBMA-BSA NPs can also contribute for their improved uptake (as analysed in section 3.2.). In fact, in culture medium supplemented with FBS, the IR/BSA NPs not only presented a negative surface charge (Table 1) but also suffered an up to 4-fold increase in their size distribution (Figure 3), which may contribute for their lower cellular uptake.

Finally, the phototherapeutic capacity of IR/SBMA-BSA NPs towards MCF-7 cells was investigated. At the concentration of 2 μg mL^{-1} (of IR780 equivalents), the non-irradiated IR/SBMA-BSA NPs could decrease MCF-7 cells' viability to 81 % (Figure 6(D)), while the combined action of IR/SBMA-BSA NPs and NIR light (808 nm, 1.7 W cm^{-2}, 5 min) decreased the cells' viability to 63 %. In contrast, the combination of NIR light and IR/SBMA-BSA NPs, at the concentration of 5 μg mL^{-1}, generated an improved therapeutic effect by further decreasing MCF-7 cells' viability to about 12 %. In these assays, the sole application of the NIR light did not cause cytotoxicity, which is in agreement with the weak interaction of this radiation with biological components as well as with our previous reports (Alves et al., 2019; de Melo-Diogo et al., 2017a; Moreira et al., 2018; Rodrigues et al., 2019).

Rajendrakumar *et al.* prepared IR780 loaded poly(12-(methacryloyloxy)dodecyl phosphorylcholine) micelles that, at the concentration of 15 μg mL^{-1} (of IR780 equivalents), could reduce cancer cells' viability to 20 % upon NIR laser irradiation (808 nm, 2.0 W cm^{-2}, 5 min) (Rajendrakumar et al., 2018). In our previous work, the chemo-phototherapeutic effect mediated by IR780 and DOX loaded hyaluronic acid-based micelles reduced MCF-7 cells' viability to about 20 % (3.5 μg mL^{-1} of IR780; 1.93 μg mL^{-1} of DOX; 808 nm, 1.7 W cm^{-2}, 5 min) (Alves et al., 2019). Herein, the phototherapeutic effect (808 nm, 1.7 W cm^{-2}, 5 min) induced by IR/SBMA-BSA NPs decreased MCF-7 cells' viability to 12 % at only 5 μg mL^{-1} (of IR780 equivalents). In this way, IR/SBMA-BSA NPs are promising agents for breast cancer phototherapy.

4. Conclusion

In this work, IR780 loaded SBMA functionalized BSA NPs were prepared for the first time for application in breast cancer phototherapy. The IR/SBMA-BSA NPs presented a spherical morphology with a size of 96.1 ± 8.1 nm. When compared to the non-functionalized BSA nanoparticles loaded with IR780 (IR/BSA NPs), the IR/SBMA-BSA NPs presented a neutral surface charge in biologically relevant media, which was attributed to the SBMA-functionalization. The IR/SBMA-BSA NPs also displayed an improved stability when dispersed in PBS and DMEM-F12 supplemented with FBS, while the IR/BSA NPs suffered an up to 4-fold increase in their size. Due to their neutral surface charge and improved colloidal stability, the IR/SBMA-BSA NPs could achieve a 1.9-fold higher uptake by MCF-7 cells when compared to IR/BSA NPs. Furthermore, the IR/SBMA-BSA NPs were cytocompatible towards NHDF, while they were able to reduce MCF-7 cells' viability up to 42 %, which can be justified by IR780 higher mitochondrial accumulation in cancer cells. The combined action of NIR light and IR/SBMA-BSA NPs could further reduce MCF-7 cells' viability to about 12 %. Overall, the SBMA-functionalized BSA nanoparticles incorporating IR780 have enhanced properties for application in breast cancer phototherapy. In the future, SBMA-*g*-BSA NPs with different SBMA functionalizations may be prepared in order to disclose the optimal SBMA grafting degree. Furthermore, *in vivo* assays will be performed to determine the blood stability, biodistribution and immunogenicity of the IR/SBMA-BSA NPs.

Conflict of interest

Declarations of interest: none.

Acknowledgments

This work was supported by FEDER funds through the POCI – COMPETE 2020 – Operational Programme Competitiveness and Internationalisation in Axis I – Strengthening research, technological development and innovation (Project POCI-01-0145-FEDER-007491) and National Funds by FCT – Foundation for

Science and Technology (Project UID/Multi/00709/2013). The funding from CENTRO-01-0145-FEDER-028989 and POCI-01-0145-FEDER-031462 is also acknowledged. Duarte de Melo-Diogo acknowledges CENTRO-01-0145-FEDER-028989 for the funding given on the form of a research contract. Cátia G. Alves and Rita Lima-Sousa acknowledge individual PhD fellowships from FCT (SFRH/BD/145386/2019 and SFRH/BD/144922/2019).

5. References

Abu Lila, A.S., Kiwada, H., Ishida, T., 2013a. The accelerated blood clearance (ABC) phenomenon: Clinical challenge and approaches to manage. J. Controlled Release 172, 38-47. https://doi.org/10.1016/j.jconrel.2013.07.026.

Abu Lila, A.S., Nawata, K., Shimizu, T., Ishida, T., Kiwada, H., 2013b. Use of polyglycerol (PG), instead of polyethylene glycol (PEG), prevents induction of the accelerated blood clearance phenomenon against long-circulating liposomes upon repeated administration. Int. J. Pharm. (Amsterdam, Neth.) 456, 235-242. https://doi.org/10.1016/j.ijpharm.2013.07.059.

Alves, C.G., de Melo-Diogo, D., Lima-Sousa, R., Costa, E.C., Correia, I.J., 2019. Hyaluronic acid functionalized nanoparticles loaded with IR780 and DOX for cancer chemo-photothermal therapy. Eur. J. Pharm. Biopharm. 137, 86-94. https://doi.org/10.1016/j.ejpb.2019.02.016.

Alves, C.G., Lima-Sousa, R., de Melo-Diogo, D., Louro, R.O., Correia, I.J., 2018. IR780 based nanomaterials for cancer imaging and photothermal, photodynamic and combinatorial therapies. Int. J. Pharm. (Amsterdam, Neth.) 542, 164-175. https://doi.org/10.1016/j.ijpharm.2018.03.020.

An, F.-F., Zhang, X.-H., 2017. Strategies for preparing albumin-based nanoparticles for multifunctional bioimaging and drug delivery. Theranostics 7, 3667-3689. https://www.thno.org/v07p3667.htm.

Bae, S., Ma, K., Kim, T.H., Lee, E.S., Oh, K.T., Park, E.-S., Lee, K.C., Youn, Y.S., 2012. Doxorubicin-loaded human serum albumin nanoparticles surface-modified with TNF-related apoptosis-inducing ligand and transferrin for targeting multiple tumor types. Biomaterials 33, 1536-1546. https://doi.org/10.1016/j.biomaterials.2011.10.050.

Blanco, E., Shen, H., Ferrari, M., 2015. Principles of nanoparticle design for overcoming biological barriers to drug delivery. Nat. Biotechnol. 33, 941-951. https://doi.org/10.1038/nbt.3330.

Chang, Y., Chen, S., Zhang, Z., Jiang, S., 2006. Highly protein-resistant coatings from well-defined diblock copolymers containing sulfobetaines. Langmuir 22, 2222-2226. https://doi.org/10.1021/la052962v.

Chen, L., Tan, L., Liu, S., Bai, L., Wang, Y., 2014. Surface modification by grafting of poly (SBMA-co-AEMA)-g-PDA coating and its application in CE. J. Biomater. Sci., Polym. Ed. 25, 766-785. https://doi.org/10.1080/09205063.2014.905030.

Chithrani, D.B., 2010. Intracellular uptake, transport, and processing of gold nanostructures. Mol. Membr. Biol. 27, 299-311. https://doi.org/10.3109/09687688.2010.507787.

d'Avanzo, N., Celia, C., Barone, A., Di Marzio, L., Santos, H.A., Fresta, M., 2019. Immunogenicity of Polyethylene glycol Based Nanomedicines: Mechanisms, Clinical Implications and Systematic Approach. Advanced Therapeutics.

de Melo-Diogo, D., Costa, E.C., Alves, C.G., Lima-Sousa, R., Ferreira, P., Louro, R.O., Correia, I.J., 2018. POxylated graphene oxide nanomaterials for combination chemo-phototherapy of breast cancer cells. Eur. J. Pharm. Biopharm. 131, 162-169. https://doi.org/10.1016/j.ejpb.2018.08.008.

de Melo-Diogo, D., Pais-Silva, C., Costa, E.C., Louro, R.O., Correia, I.J., 2017a. D-α-tocopheryl polyethylene glycol 1000 succinate functionalized nanographene oxide for cancer therapy. Nanomedicine (London, U. K.) 12, 443-456. https://doi.org/10.2217/nnm-2016-0384.

de Melo-Diogo, D., Pais-Silva, C., Dias, D.R., Moreira, A.F., Correia, I.J., 2017b. Strategies to Improve Cancer Photothermal Therapy Mediated by Nanomaterials. Adv. Healthcare Mater. 6. https://doi.org/10.1002/adhm.201700073.

Dong, Z., Mao, J., Yang, M., Wang, D., Bo, S., Ji, X., 2011. Phase behavior of poly (sulfobetaine methacrylate)-grafted silica nanoparticles and their stability in protein solutions. Langmuir 27, 15282-15291. https://doi.org/10.1021/la2038558.

Guo, F., Yu, M., Wang, J., Tan, F., Li, N., 2016. The mitochondria-targeted and IR780-regulated theranosomes for imaging and enhanced photodynamic/photothermal therapy. RSC Adv. 6, 11070-11076. 10.1039/c5ra19521g.

Hobbs, S.K., Monsky, W.L., Yuan, F., Roberts, W.G., Griffith, L., Torchilin, V.P., Jain, R.K., 1998. Regulation of transport pathways in tumor vessels: Role of tumor type and microenvironment. Proc. Natl. Acad. Sci. U. S. A. 95, 4607-4612. https://doi.org/10.1073/pnas.95.8.4607.

Ibrahim, G.S., Isloor, A.M., Asiri, A.M., Ismail, N., Ismail, A.F., Ashraf, G.M., 2017. Novel, one-step synthesis of zwitterionic polymer nanoparticles via distillation-

precipitation polymerization and its application for dye removal membrane. Sci. Rep. 7, 15889. https://doi.org/10.1038/s41598-017-16131-9.

Jiang, C., Cheng, H., Yuan, A., Tang, X., Wu, J., Hu, Y., 2015. Hydrophobic IR780 encapsulated in biodegradable human serum albumin nanoparticles for photothermal and photodynamic therapy. Acta Biomater. 14, 61-69. https://doi.org/10.1016/j.actbio.2014.11.041.

Kim, B., Lee, C., Lee, E.S., Shin, B.S., Youn, Y.S., 2016. Paclitaxel and curcumin co-bound albumin nanoparticles having antitumor potential to pancreatic cancer. Asian J. Pharm. Sci. 11, 708-714. https://doi.org/10.1016/j.ajps.2016.05.005.

Kirui, D.K., Rey, D.A., Batt, C.A., 2010. Gold hybrid nanoparticles for targeted phototherapy and cancer imaging. Nanotechnology 21, 105105. https://doi.org/10.1088/0957-4484/21/10/105105.

Ladd, J., Zhang, Z., Chen, S., Hower, J.C., Jiang, S., 2008. Zwitterionic polymers exhibiting high resistance to nonspecific protein adsorption from human serum and plasma. Biomacromolecules 9, 1357-1361. https://doi.org/10.1021/bm701301s.

Leitão, M.M., de Melo-Diogo, D., Alves, C.G., Lima-Sousa, R., Correia, I.J., 2020. Prototypic Heptamethine Cyanine Incorporating Nanomaterials for Cancer Phototheragnostic. Adv. Healthcare Mater. 9, 1901665. 10.1002/adhm.201901665.

Lima-Sousa, R., de Melo-Diogo, D., Alves, C.G., Costa, E.C., Ferreira, P., Louro, R.O., Correia, I.J., 2018. Hyaluronic acid functionalized green reduced graphene oxide for targeted cancer photothermal therapy. Carbohydr. Polym. 200, 93-99. https://doi.org/10.1016/j.carbpol.2018.07.066.

Liu, H., Wang, K., Yang, C., Huang, S., Wang, M., 2017. Multifunctional polymeric micelles loaded with doxorubicin and poly(dithienyl-diketopyrrolopyrrole) for near-infrared light-controlled chemo-phototherapy of cancer cells. Colloids Surf., B 157, 398-406. https://doi.org/10.1016/j.colsurfb.2017.05.080.

Liu, X., Tao, H., Yang, K., Zhang, S., Lee, S.-T., Liu, Z., 2011. Optimization of surface chemistry on single-walled carbon nanotubes for in vivo photothermal ablation of tumors. Biomaterials 32, 144-151. https://doi.org/10.1016/j.biomaterials.2010.08.096.

Lou, S., Zhang, X., Zhang, M., Ji, S., Wang, W., Zhang, J., Li, C., Kong, D., 2017. Preparation of a dual cored hepatoma-specific star glycopolymer nanogel via

arm-first ATRP approach. Int. J. Nanomed. 12, 3653-3664. https://doi.org/10.2147/IJN.S134367.

Lu, I.-L., Liu, T.-I., Lin, H.-C., Chang, S.-H., Lo, C.-L., Chiang, W.-H., Chiu, H.-C., 2019. IR780-loaded zwitterionic polymeric nanoparticles with acidity-induced agglomeration for enhanced tumor retention. Eur. Polym. J., 109400. https://doi.org/10.1016/j.eurpolymj.2019.109400.

Matsumoto, Y., Nichols, J.W., Toh, K., Nomoto, T., Cabral, H., Miura, Y., Christie, R.J., Yamada, N., Ogura, T., Kano, M.R., Matsumura, Y., Nishiyama, N., Yamasoba, T., Bae, Y.H., Kataoka, K., 2016. Vascular bursts enhance permeability of tumour blood vessels and improve nanoparticle delivery. Nat. Nanotechnol. 11, 533-538. https://doi.org/10.1038/nnano.2015.342.

Men, Y., Peng, S., Yang, P., Jiang, Q., Zhang, Y., Shen, B., Dong, P., Pang, Z., Yang, W., 2018. Biodegradable zwitterionic nanogels with long circulation for antitumor drug delivery. ACS Appl. Mater. Interfaces 10, 23509-23521. https://doi.org/10.1021/acsami.8b03943.

Moreira, A.F., Rodrigues, C.F., Reis, C.A., Costa, E.C., Ferreira, P., Correia, I.J., 2018. Development of poly-2-ethyl-2-oxazoline coated gold-core silica shell nanorods for cancer chemo-photothermal therapy. Nanomedicine (London, U. K.) 13, 2611-2627. https://doi.org/10.2217/nnm-2018-0179.

Muro, E., Pons, T., Lequeux, N., Fragola, A., Sanson, N., Lenkei, Z., Dubertret, B., 2010. Small and stable sulfobetaine zwitterionic quantum dots for functional live-cell imaging. J. Am. Chem. Soc. 132, 4556-4557.

Nikam, D.S., Jadhav, S.V., Khot, V.M., Ningthoujam, R., Hong, C.K., Mali, S.S., Pawar, S., 2014. Colloidal stability of polyethylene glycol functionalized Co 0.5 Zn 0.5 Fe 2 O 4 nanoparticles: effect of pH, sample and salt concentration for hyperthermia application. RSC Adv. 4, 12662-12671.

Otsuka, H., Nagasaki, Y., Kataoka, K., 2012. PEGylated nanoparticles for biological and pharmaceutical applications. Adv. Drug Delivery Rev. 64, 246-255. https://doi.org/10.1016/j.addr.2012.09.022.

Pais-Silva, C., de Melo-Diogo, D., Correia, I.J., 2017. IR780-loaded TPGS-TOS micelles for breast cancer photodynamic therapy. Eur. J. Pharm. Biopharm. 113, 108-117. https://doi.org/10.1016/j.ejpb.2017.01.002.

Peng, S., Ouyang, B., Men, Y., Du, Y., Cao, Y., Xie, R., Pang, Z., Shen, S., Yang, W., 2020. Biodegradable zwitterionic polymer membrane coating endowing

nanoparticles with ultra-long circulation and enhanced tumor photothermal therapy. Biomaterials 231, 119680. https://doi.org/10.1016/j.biomaterials.2019.119680.

Prencipe, G., Tabakman, S.M., Welsher, K., Liu, Z., Goodwin, A.P., Zhang, L., Henry, J., Dai, H., 2009. PEG branched polymer for functionalization of nanomaterials with ultralong blood circulation. J. Am. Chem. Soc. 131, 4783-4787. https://doi.org/10.1021/ja809086q.

Rajendrakumar, S., Chang, N.-C., Mohapatra, A., Uthaman, S., Lee, B.-I., Tsai, W.-b., Park, I.-K., 2018. A lipophilic ir-780 dye-encapsulated zwitterionic polymer-lipid micellar nanoparticle for enhanced photothermal therapy and nir-based fluorescence imaging in a cervical tumor mouse model. Int. J. Mol. Sci. 19, 1189. https://doi.org/10.3390/ijms19041189.

Reis, C.A., Rodrigues, C.F., Moreira, A.F., Jacinto, T.A., Ferreira, P., Correia, I.J., 2019. Development of gold-core silica shell nanospheres coated with poly-2-ethyl-oxazoline and β-cyclodextrin aimed for cancer therapy. Mater. Sci. Eng. C 98, 960-968. https://doi.org/10.1016/j.msec.2019.01.068.

Rodrigues, C.F., Reis, C.A., Moreira, A.F., Ferreira, P., Correia, I.J., 2019. Optimization of gold core-mesoporous silica shell functionalization with TPGS and PEI for cancer therapy. Microporous Mesoporous Mater. 285, 1-12. https://doi.org/10.1016/j.micromeso.2019.04.064.

Sheng, Y., Yuan, Y., Liu, C., Tao, X., Shan, X., Xu, F., 2009. In vitro macrophage uptake and in vivo biodistribution of PLA–PEG nanoparticles loaded with hemoglobin as blood substitutes: effect of PEG content. J. Mater. Sci.: Mater. Med. 20, 1881-1891. https://doi.org/10.1007/s10856-009-3746-9.

Shiraishi, K., Hamano, M., Ma, H., Kawano, K., Maitani, Y., Aoshi, T., Ishii, K.J., Yokoyama, M., 2013. Hydrophobic blocks of PEG-conjugates play a significant role in the accelerated blood clearance (ABC) phenomenon. J. Controlled Release 165, 183-190. https://doi.org/10.1016/j.jconrel.2012.11.016.

Shutava, T.G., Livanovich, K.S., Pankov, V.V., 2018. Synergetic effect of polyethylene glycol-grafted chitosan and bovine serum albumin on colloidal stability of polyelectrolyte nanocapsules. Colloids and Surfaces A: Physicochemical and Engineering Aspects 539, 69-79.

Spence, A., Simpson, A.J., Mcnally, D.J., Moran, B.W., McCaul, M.V., Hart, K., Paull, B., Kelleher, B.P., 2011. The degradation characteristics of microbial biomass in soil. Geochimica et Cosmochimica Acta 75, 2571-2581.

Venault, A., Yang, H.-S., Chiang, Y.-C., Lee, B.-S., Ruaan, R.-C., Chang, Y., 2014. Bacterial resistance control on mineral surfaces of hydroxyapatite and human teeth via surface charge-driven antifouling coatings. ACS Appl. Mater. Interfaces 6, 3201-3210. https://doi.org/10.1021/am404780w.

Wang, K., Zhang, Y., Wang, J., Yuan, A., Sun, M., Wu, J., Hu, Y., 2016. Self-assembled IR780-loaded transferrin nanoparticles as an imaging, targeting and PDT/PTT agent for cancer therapy. Sci. Rep. 6, 27421. https://doi.org/10.1038/srep27421.

Wang, Y., Liu, T., Zhang, E., Luo, S., Tan, X., Shi, C., 2014. Preferential accumulation of the near infrared heptamethine dye IR-780 in the mitochondria of drug-resistant lung cancer cells. Biomaterials 35, 4116-4124. https://doi.org/10.1016/j.biomaterials.2014.01.061.

Wilhelm, S., Tavares, A.J., Dai, Q., Ohta, S., Audet, J., Dvorak, H.F., Chan, W.C.W., 2016. Analysis of nanoparticle delivery to tumours. Nat. Rev. Mater. 1, 16014. https://doi.org/10.1038/natrevmats.2016.14.

Xia, B., Zhang, W., Shi, J., Xiao, S.-j., 2013. Engineered stealth porous silicon nanoparticles via surface encapsulation of bovine serum albumin for prolonging blood circulation in vivo. ACS Appl. Mater. Interfaces 5, 11718-11724. https://doi.org/10.1021/am403380e.

Xu, H., Wang, K.Q., Deng, Y.H., Chen, D.W., 2010. Effects of cleavable PEG-cholesterol derivatives on the accelerated blood clearance of PEGylated liposomes. Biomaterials 31, 4757-4763. https://doi.org/10.1016/j.biomaterials.2010.02.049.

Yan, L., Zhao, F., Wang, J., Zu, Y., Gu, Z., Zhao, Y., 2019. A Safe-by-Design Strategy towards Safer Nanomaterials in Nanomedicines. Adv. Mater. 31, 1805391. https://doi.org/10.1002/adma.201805391.

Yuan, A., Qiu, X., Tang, X., Liu, W., Wu, J., Hu, Y., 2015. Self-assembled PEG-IR-780-C13 micelle as a targeting, safe and highly-effective photothermal agent for in vivo imaging and cancer therapy. Biomaterials 51, 184-193. https://doi.org/10.1016/j.biomaterials.2015.01.069.

Zhang, C., Liu, T., Su, Y., Luo, S., Zhu, Y., Tan, X., Fan, S., Zhang, L., Zhou, Y., Cheng, T., 2010. A near-infrared fluorescent heptamethine indocyanine dye with preferential tumor accumulation for in vivo imaging. Biomaterials 31, 6612-6617. https://doi.org/10.1016/j.biomaterials.2010.05.007.

Zhang, K., Fang, H., Chen, Z., Taylor, J.-S.A., Wooley, K.L., 2008. Shape effects of nanoparticles conjugated with cell-penetrating peptides (HIV Tat PTD) on CHO cell uptake. Bioconjugate Chem. 19, 1880-1887. https://doi.org/10.1021/bc800160b.

Zhou, M., Zhang, R., Huang, M., Lu, W., Song, S., Melancon, M.P., Tian, M., Liang, D., Li, C., 2010. A chelator-free multifunctional [64Cu] CuS nanoparticle platform for simultaneous micro-PET/CT imaging and photothermal ablation therapy. J. Am. Chem. Soc. 132, 15351-15358. https://doi.org/10.1021/ja106855m.

Zou, W., Fan, Z., Zhai, S., Wang, S., Xu, B., Cai, Z., 2020. A multifunctional antifog, antifrost, and self-cleaning zwitterionic polymer coating based on poly (SBMA-co-AA). Journal of Coatings Technology and Research, 1-12.

Figure Captions

Fig. 1 – Synthesis and characterization of SBMA-*g*-BSA. Schematic representation of the polymer synthesis (A). FTIR spectra of SBMA, BSA and SBMA-*g*-BSA (B). FTIR spectrum of SBMA-*g*-BSA in the 1800-600 cm^{-1} wavenumber range (C). ^{1}H NMR spectra of SBMA (D), BSA (E) and SBMA-*g*-BSA (F).

Fig. 2 – Formulation and characterization of IR/SBMA-BSA NPs. Schematic representation of the nanoparticles' formulation and phototherapeutic application (A). DLS size distribution (B) and TEM analysis (C) of IR/SBMA-BSA NPs. Scale bar corresponds to 200 nm.

Fig. 3 – Stability of IR/SBMA-BSA and IR/BSA NPs in different media. Size variation of IR/SBMA-BSA and IR/BSA NPs when dispersed in PBS (pH 7.4) at 10 mM (of Na_2HPO_4) (A), in DMEM-F12 medium with 0 % (B), 10 % (C), and 20 % (D) of FBS (v/v). The values of each group were normalized using the respective initial size (t = 0 h). Each bar represents mean ± S.D. (n = 3).

Fig. 4 – Evaluation of the photothermal capacity of IR/SBMA-BSA NPs. UV-Vis-NIR absorption spectra of free IR780 (2.5 μg mL^{-1}; in methanol) and of IR/SBMA-BSA NPs (at 2.5 μg mL^{-1} of IR780 equivalents) (A). UV-Vis-NIR absorption spectra of IR/SBMA-BSA NPs in PBS (B) and in DMEM-F12 medium supplemented with 10 % of FBS (C) after 0 and 24 h of incubation. *In vitro* temperature increase mediated by IR/SBMA-BSA NPs, at different concentrations of IR780 equivalents, upon NIR laser irradiation (808 nm, 1.7 W cm^{-2}) (D).

Fig. 5 – Cytocompatibility of IR/SBMA-BSA NPs. Cytocompatibility of IR/SBMA-BSA NPs at different concentrations (of IR780 equivalents) and incubation times

(24 and 48 h) towards MCF-7 cells (A) and NHDF (B). K- and K+ were used as negative and positive controls, respectively. Each bar represents the mean ± SD (n = 5).

Fig. 6 – *In vitro* biological evaluation of IR/SBMA-BSA NPs. Uptake of IR/SBMA-BSA NPs and IR/BSA NPs by MCF-7 cells when incubated using DMEM-F12 medium with 0 % (A), 10 % (B), and 20 % (C) of FBS (v/v). The fluorescence values were normalized using the fluorescence values obtained for cells incubated with IR/BSA NPs. Evaluation of the therapeutic effect mediated by IR/SBMA-BSA NPs, at different concentrations (of IR780 equivalents), upon NIR laser irradiation (808 nm, 1.7 W cm^{-2}, 5 min) towards MCF-7 cells (D). K- and K+ were used as negative and positive controls, respectively. Each bar represents the mean ± SD (n = 5), *$p < 0.05$.

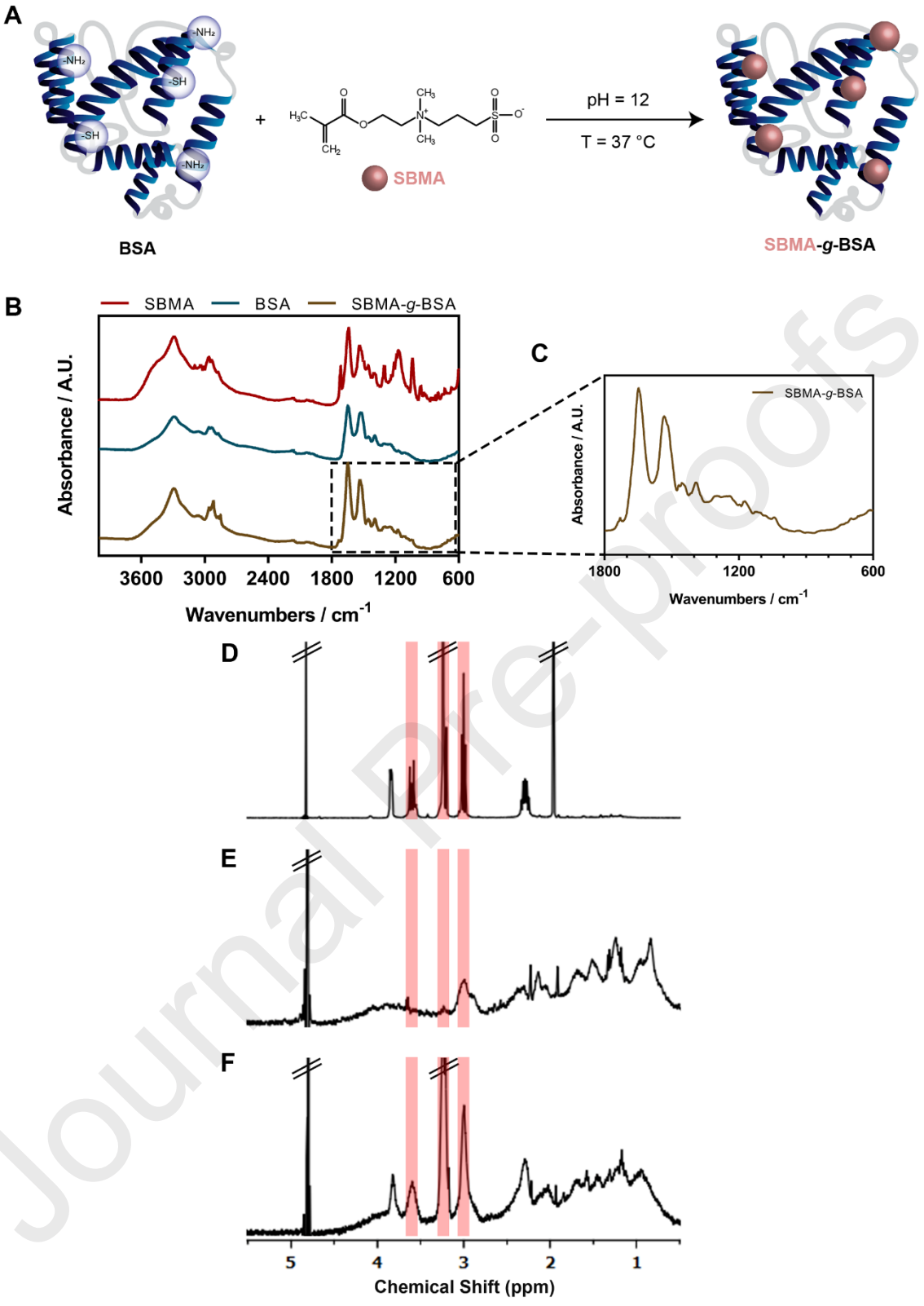

Figure 1

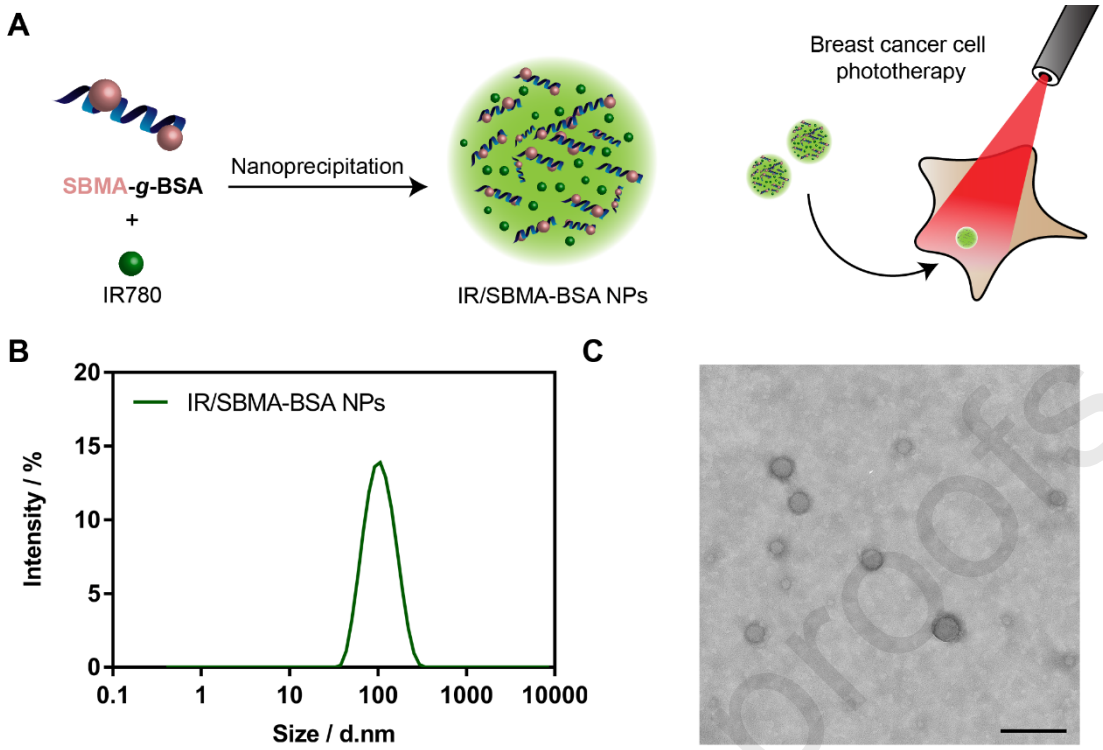

Figure 2

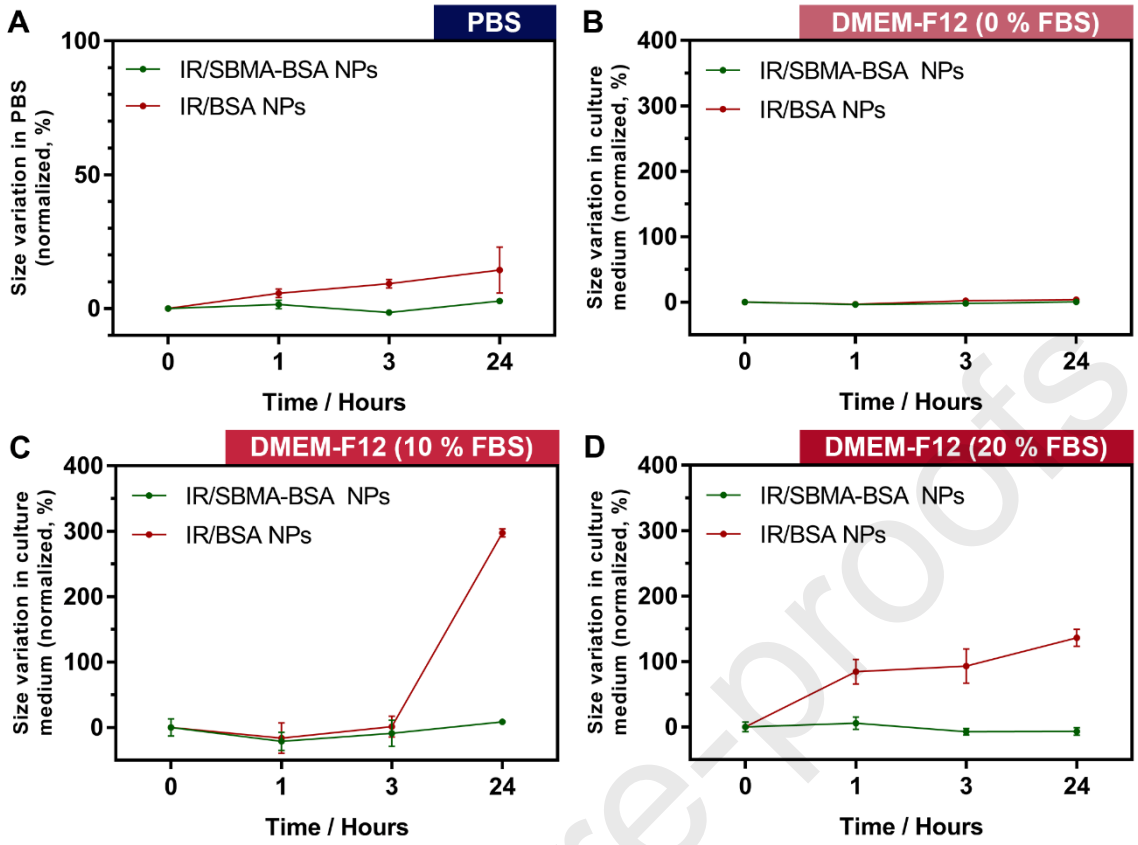

Figure 3

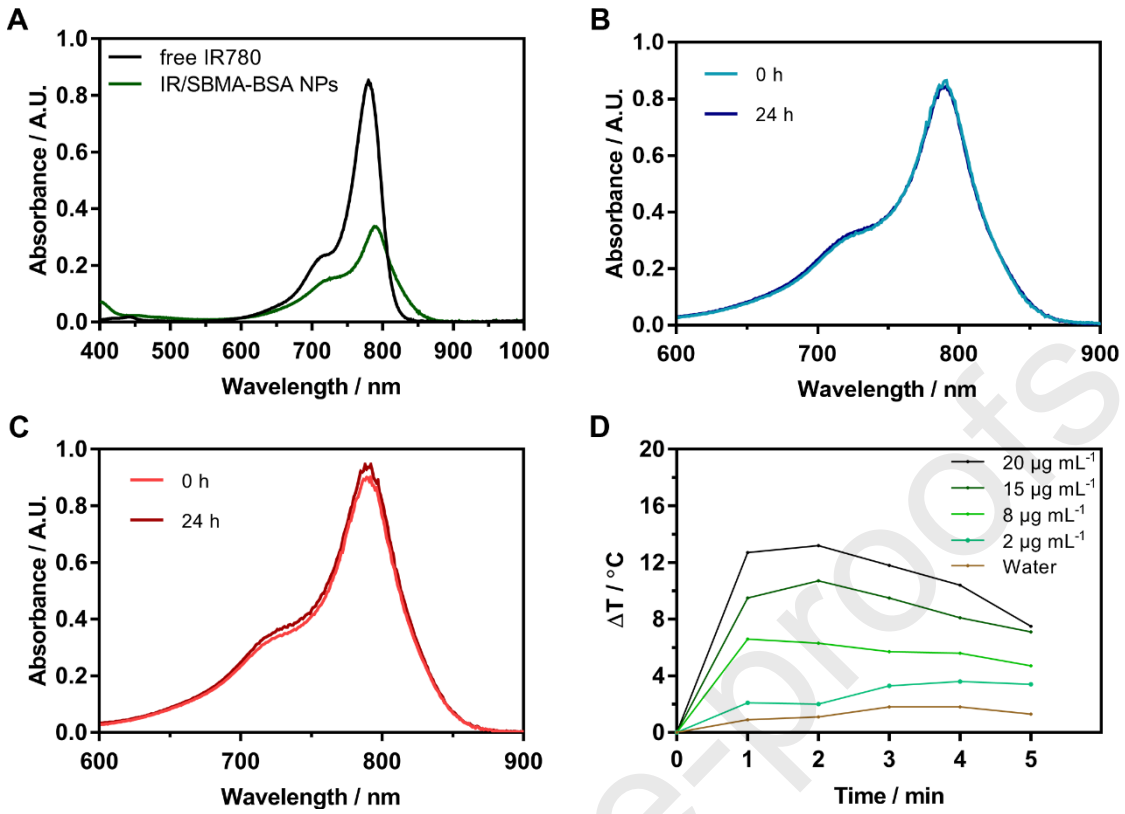

Figure 4

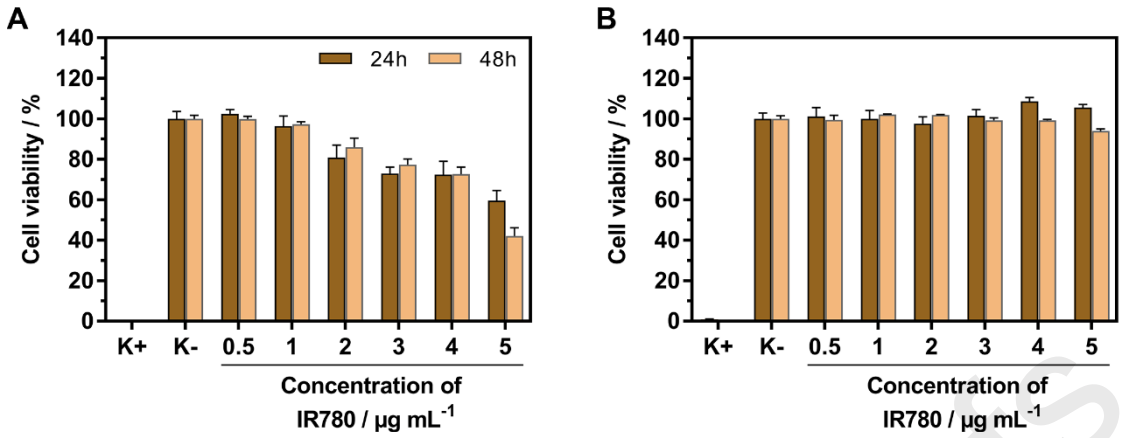

Figure 5

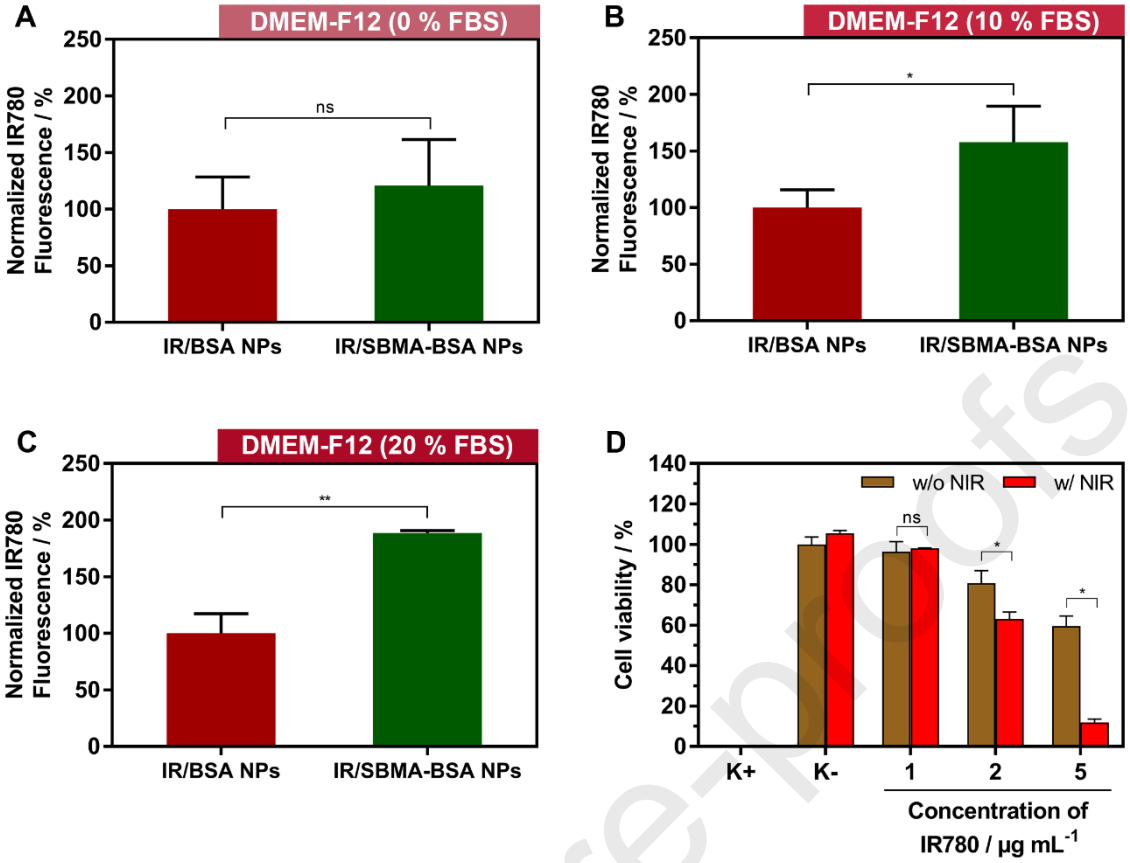

Figure 6

Table 1 - Zeta potential of IR/SBMA-BSA NPs and IR/BSA NPs in different media.

Solvent	IR/SBMA-BSA NPs zeta potential (mV)	IR/BSA NPs zeta potential (mV)
Water	-18.83 ± 0.61	-24.75 ± 0.49
PBS 5 mM* (pH 7.4)	-11.30 ± 0.57	-13.87 ± 0.86
PBS 10 mM* (pH 7.4)	-9.60 ± 0.47	-12.33 ± 1.22
Culture medium with 0 % of FBS	-9.78 ± 0.73	-12.23 ± 1.29
Culture medium with 10 % of FBS	-9.04 ± 0.94	-11.73 ± 0.99
Culture medium with 20 % of FBS	-6.34 ± 0.33	-10.17 ± 1.88

*concentration of Na_2HPO_4

Table 1 - Zeta potential of IR/SBMA-BSA NPs and IR/BSA NPs in different media.

Solvent	IR/SBMA-BSA NPs zeta potential (mV)	IR/BSA NPs zeta potential (mV)
Water	-18.83 ± 0.61	-24.75 ± 0.49
PBS 5 mM* (pH 7.4)	-11.30 ± 0.57	-13.87 ± 0.86
PBS 10 mM* (pH 7.4)	-9.60 ± 0.47	-12.33 ± 1.22
Culture medium with 0 % of FBS	-9.78 ± 0.73	-12.23 ± 1.29
Culture medium with 10 % of FBS	-9.04 ± 0.94	-11.73 ± 0.99
Culture medium with 20 % of FBS	-6.34 ± 0.33	-10.17 ± 1.88

*concentration of Na_2HPO_4

Cátia G. Alves: Investigation, Formal analysis and Writing- Original draft preparation

Duarte de Melo-Diogo: Conceptualization, Investigation, Supervision, Writing- Reviewing and Editing

Rita Lima-Sousa: Investigation

Ilídio J. Correia: Project administration, Funding acquisition, Supervision, Writing- Reviewing and Editing

Declaration of interests

☒ The authors declare that they have no known competing financial interests or personal relationships that could have appeared to influence the work reported in this paper.

☐The authors declare the following financial interests/personal relationships which may be considered as potential competing interests:

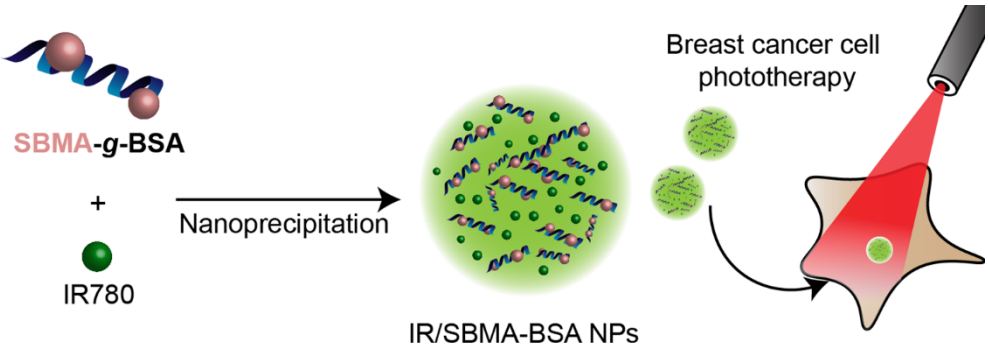

Highlights

- Novel IR780 loaded SBMA-functionalized BSA NPs (IR/SBMA-BSA NPs) were produced
- SBMA-functionalization yielded IR/SBMA-BSA NPs displaying a neutral surface charge
- IR/SBMA-BSA NPs displayed an improved stability in biological relevant media
- IR/SBMA-BSA NPs achieved a 1.9-fold higher uptake by MCF-7 cells
- IR/SBMA-BSA NPs interaction with NIR light enhanced the therapeutic outcome